INTERNATIONAL SOCIETY FOR
SOIL MECHANICS AND
GEOTECHNICAL ENGINEERING

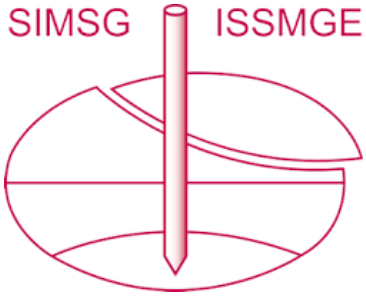

This paper was downloaded from the Online Library of the International Society for Soil Mechanics and Geotechnical Engineering (ISSMGE). The library is available here:

https://www.issmge.org/publications/online-library

This is an open-access database that archives thousands of papers published under the Auspices of the ISSMGE and maintained by the Innovation and Development Committee of ISSMGE.

The paper was published in the proceedings of the 6th International Conference on Geotechnical and Geophysical Site Characterization and was edited by Tamás Huszák, András Mahler and Edina Koch. The conference was originally scheduled to be held in Budapest, Hungary in 2020, but due to the COVID-19 pandemic, it was held online from September 26th to September 29th 2021.

Large scale & efficient geotechnical soil investigations: Applying machine learning on airborne geophysical models to map sensitive glaciomarine clay

Craig William Christensen[1], Andreas Aspmo Pfaffhuber[2], Guro Huun Skurdal[3]
EMerald Geomodelling, Oslo, Norway, cch@emeraldgeo.com[1], aap@emeraldgeo.com[2], ghs@emeraldgeo.com[3]

Asgeir Olof Kydland Lysdahl[1], Malte Vöge
Norwegian Geotechnical Institute, Oslo, Norway, aol@ngi.no[1], mvo@ngi.no[2]

ABSTRACT: Globally, 90% of large infrastructure projects report cost overruns of 20 to 50% for linear structures. Uncertainties in ground conditions are the most common reason for overruns and delays. Intrusive geotechnical soil investigations are too costly and time consuming to provide seamless coverage. Geophysical methods can fill data gaps quickly but these data can be difficult to interpret. We translate complicated geophysical models into useful engineering parameters by using machine learning-based interpretation that accounts for geotechnical information. In this paper, we illustrate the applicability of airborne geo-scanning for mapping sensitive clay. We first derive bedrock topography combining geophysical 3D-models with sparse bedrock elevation data from drillings. We then combine geophysics with geotechnical soundings and samples to map sensitive clay in 3D. We evaluate this method using randomized cross-validation, varying the number of training data used. Results indicate that while the predictions are imperfect, even with sparse input data, they can give early indications of where the presence of sensitive clay can be either ruled out, confirmed, or deemed uncertain. These insights can be useful for planning more efficient follow up site investigations, reducing overall risk, time and cost of a project.

Keywords: site investigation; airborne geoscanning; machine learning; bedrock topography; sensitive clay

1. Introduction

Geological risk is frequently identified as a key factor leading to significant schedule delays and cost overruns in large scale infrastructure projects like roads, railways, and tunnels [1]. In the early stages of planning, finding a suitable corridor or area to build in is critical. Large areas have to be covered to be able to see and compare the risk of choosing between surface constructions on deep, soft sediments along one route, or tunnels along another route. Conventional geotechnical ground investigation techniques are too costly and time intensive to provide full coverage over relatively large areas of interest.

Airborne geo-scanning is an emerging technology that can mitigate the geological uncertainty of these areas, and it can give engineers the tool needed to make the right choices at an early stage in big infrastructure projects. Cost overruns in mega-projects have been found to reach 20-50% of the original budgeted project costs [2], making well-informed, early-phase choices crucial. Airborne geo-scanning makes use of a well-established near-surface geophysical technique: airborne electromagnetics (AEM). This method rapidly provides a seamless overview of the geophysical properties within an area. Geotechnical applications of the method have included mapping depth to bedrock [3], mapping of sensitive clay [4] identifying major weakness zones in rock [5] and supporting contaminated mass management [6].

In the past, significant labor had to be invested to manually or semi-automatically interpret geophysical models into usable geotechnical parameters [8]. Recently, we have developed machine-learning-based methods that integrate the acquired geophysical model with sparse geotechnical soil investigations into a unified ground model [8]. Thus far, these efforts have focused on automatically detecting a single continuous interface, notably the bedrock-sediment interface [9] or base of peat [10].

For this study, we focus on sensitive glaciomarine clay, otherwise known as *quick clay*. In high latitudes, quick clay poses a unique challenge as major ground improvement methods are required for constructions in such regions. In Norway, clay is usually defined as quick at a remoulded shear strength of less than 0.5 kPa and as brittle when under 2.0 kPa. (Note that quick clay is a subset of brittle material; all quick clay is brittle, but not all brittle clay is quick.) Glaciomarine clay turns into quick clay after extensive pore water leaching by groundwater and rain-water, thus salinity is a common indicator for the probability of clay to be quick. Extensive studies on samples from sites in Norway have shown the relationship between geophysical properties (resistivity), salinity and remoulded shear strength [11].

In this paper, we present a new machine-learning-based workflow for estimating the probability of quick clay using airborne geoscanning. Using large field dataset from a past road-planning project, we evaluate performance of the new method and assess its utility for future projects.

2. Field data

Our field data comes from a proposed expansion project for the E16 highway. Extensive field investigations began in late 2012 along a 30-km segment

of highway in Nes municipality, approximately 60 km northeast of Oslo (Figure 1).

This area has post-glacial geomorphology that is typical for the eastern Norwegian lowlands. Large expanses of glaciomarine clay occur along the planned road alignment (very low electrical resistivity), some sections of which are quick (low resistivity). To a lesser extent, exposed bedrock (high electrical resistivity), moraines (high resistivity), and glaciofluvial deposits (medium resistivity) are also found. Bedrock here is largely comprised of metamorphic rock types, with some igneous rocks present in the northeastern corner of the survey area.

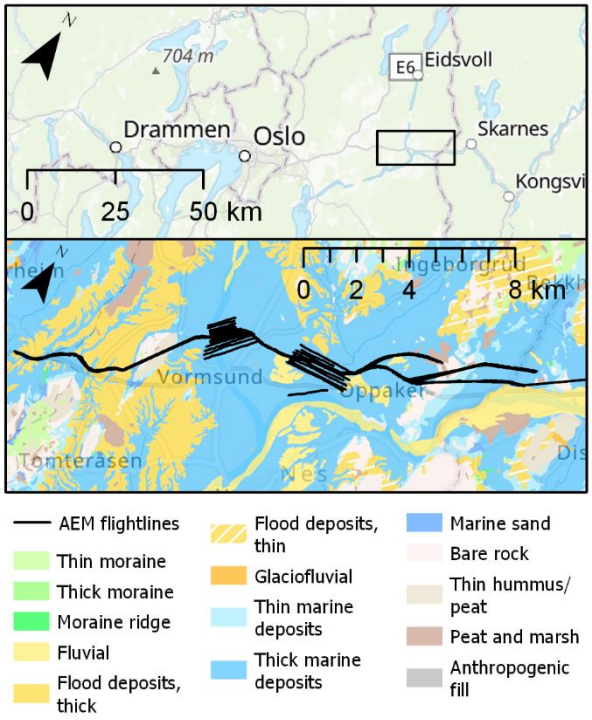

Figure 1: Overview map of the project area.

2.1. Airborne electromagnetic data

In January 2013, 178 line-km of AEM data were aquired both along the planned road alignment and on additional grids at two river crossings (Vorma to the west, and Uåa to the east). In these surveys, a helicopter towed equipment 30 m above the ground (Figure 2), specifically the SkyTEM 302 system [12]. This system measures electromagnetic induction effects between itself and the ground, a response that is dependent on the electrical resistivity of the uppermost few hundred meters of the ground.

The geophysical models that we interpret come from processed AEM survey data. First, data exhibiting noise and coupling effects were removed. Next, we used inversion modelling to produce a 3D resistivity model. Specificially, we performed spatially constrained inversion with the specialised software, Aarhus Workbench. The resulting 3D resistivity model, a portion of which is shown in Figure 3, has a vertical resolution ranging from meters close to the surface to tens of meters at larger depths. The lateral resolution is roughly 50 to 150 meters [13].

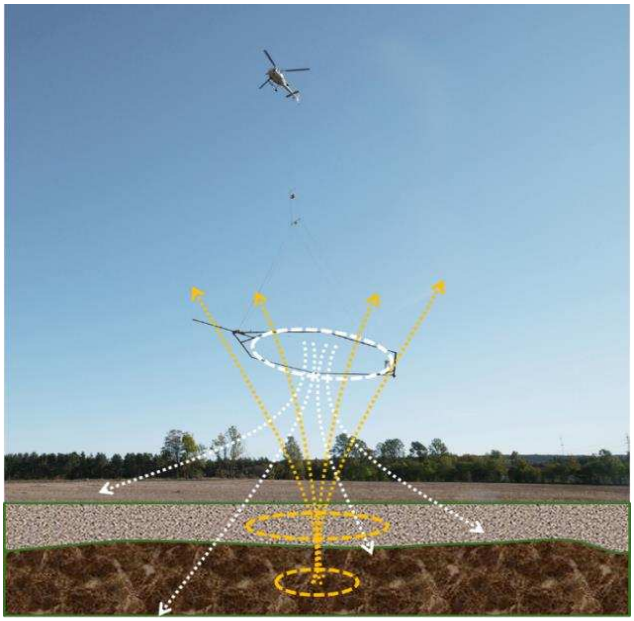

Figure 2: Illustration of the airborne electromagnetic induction principle where a primary electromagnetic pulse (white) interacts with a secondary response (yellow) that is governed by ground conditions.

2.2. Geotechnical data

Over 1300 geotechnical soundings were performed over several several years along the planned road alignment. Only 1105 had some measurement of depth to bedrock. Of these, 98 of these were total soundings which drilled at least 3 m into rock to confirm that the material was bedrock and not hard moraine or a glacial erratic. The remaining 1007 holes were rotary pressure soundings that reached a hard layer that was assumed to be bedrock.

In total, 1387 rotary pressure soundings were performed at 1379 locations. Most of these were used to investigate clay properties, with a focus on locating quick or brittle clay. Of these, 762 were within 75 m of an AEM measurement point. The drill rigs used drill rods that were 2 m long, meaning that the feed force measured decreases suddenly as a new stem is added (Fig. 4A). Between the drill stem changes, the small scale trend can differ from the large-scale trends (Fig. 4B). Occasionally, an unusually large drop in feed force occurs at a drill rod change. (Fig. 4C).

A large number of soil samples were also taken. A total of 1980 lab measurements of remolded shear strength were made at different depths in 88 different drilling locations. Over 99% of these samples where in clay material. Of these 1980, 58 were not used in the machine learning interpretation due to data quality issues, mainly because they occurred below sudden drops like those at Fig. 4C. Of these remaining 1922, roughly two thirds (1268) were non-brittle, one sixth (328) were brittle but not quick, and one sixth (326) were quick.

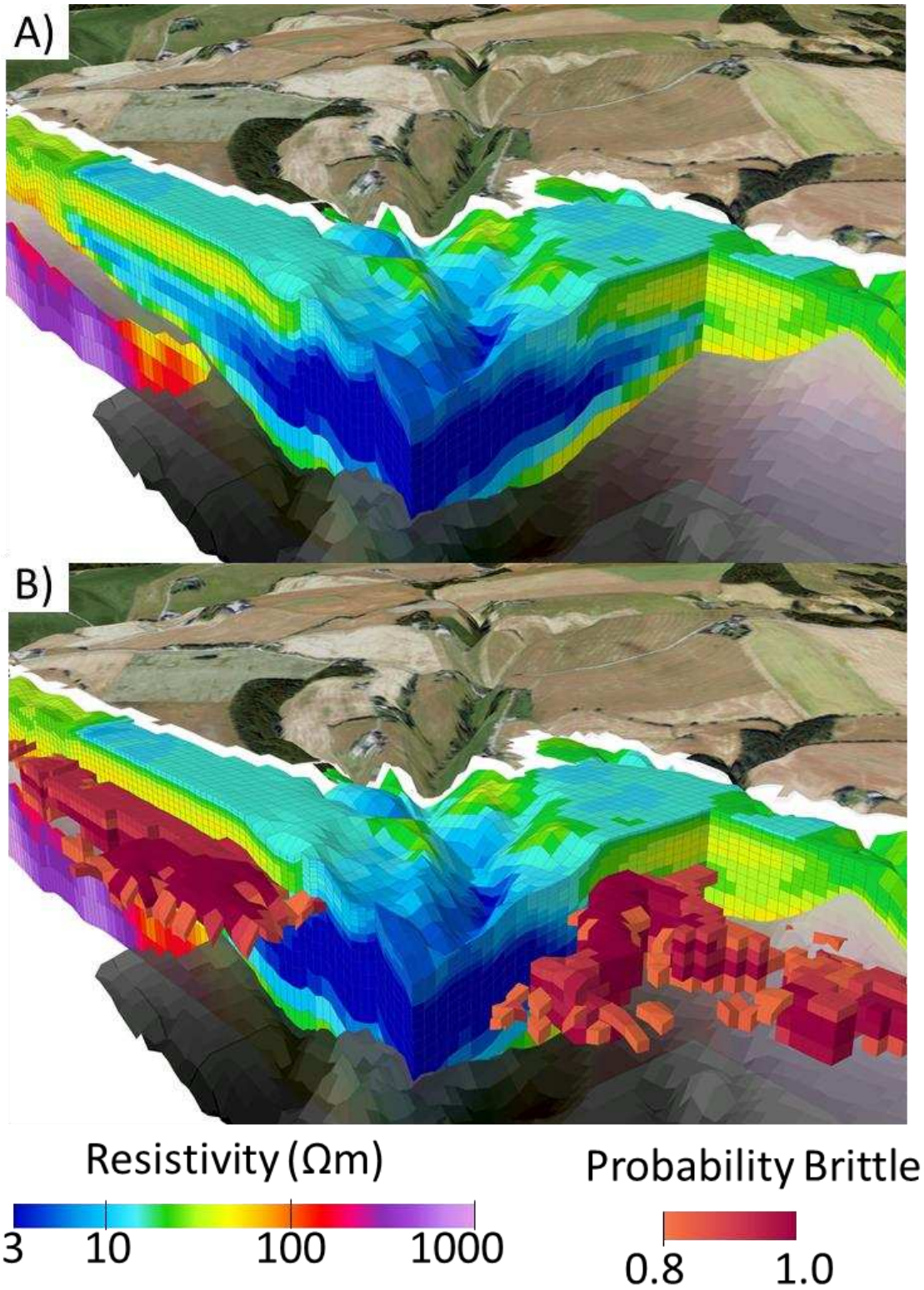

Figure 3: Three-dimensional view of some of the data and modeling outputs just west of the river Uåa, including vertical cross sections throug the AEM-derived resistivity model and the bedrock model (black and gray). Panel B also shows portions of the resistivity model in the foreground where the probability of brittle clay is very high.

3. Method

3.1. Bedrock topography

The first step in mapping quick clay occurrence is to split the resistivity model into sediment and bedrock. We use an artificial neural network (ANN) that extracts bedrock topography from the geophysical model by using existing geotechnical soundings as training data. It is based on multi-layer perceptron regression and is implemented in the "scikit-learn" Python package [14]. We have extensively tested this method in this particular field site before and refer readers to those publications for more detailed results [9]. Using this bedrock surface, we then eliminate portion of the resistivity model below bedrock from consideration in later classification. A portion of this bedrock model is shown in Figure 3.

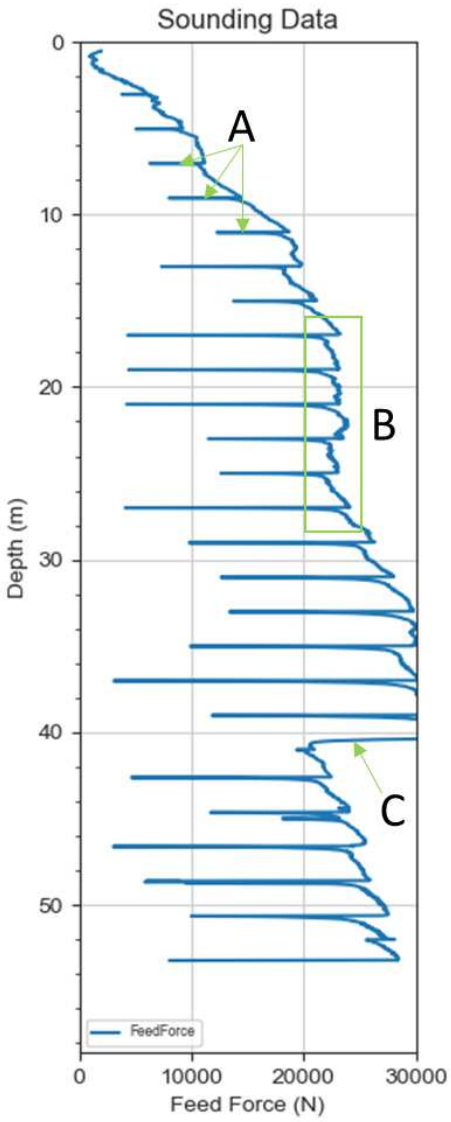

Figure 4: Example rotary pressure sounding data showing some typical features of the data: A) small, temporary dips in feed force when new drill stems are added; B) feed force between rods stems shows small scale trends (often increasing in this case) that differ from larger scale trends (often flat); C) a sudden drop in feed force after which feed force does not return to normal again.

3.2. Quick and brittle clay occurrence

3.2.1. Dataset considerations

This dataset presents three main challenges for interpreting the occurrence of quick and brittle clays. First, as with most other sites there is an imperfect relationship between remolded shear strength of clay and resistivity (Fig. 5). This is likely because marine clays can have an elevated resistivity both because of leached salts or a mix with silt and sand [11].

Second, the AEM-derived resistivity model has several weaknesses. The model layers range between 1.0 and 8.7 m thickness in the upper 40 m of the model. These resistivity values represent an estimate of volumetric average resistivity of these large blocks, a much coarser spatial resolution than the lab measurements (10 cm slugs) and geotechnical drillings (recorded at 2.5 cm intervals). The model smooths out sharp changes in resistivity, causing distortions near boundaries between material types, especially at the sediment-bedrock interface. This explains why some lab samples have a corresponding resistivity of over 1000 Ωm (Fig 5) even though quick and brittle material normally has resistivities of between 8 and 100 Ωm in Norway [15,16]. Plotting the vertical resistivity gradient reveals how smoothing causes some of these distortions (Figure 6A and B).

Lastly, the datasets sample very different ranges. Lab samples were taken almost exclusively in clay (>99%). The AEM survey in contrast samples a large volume containing multiple sediment types. Hence the range of resistivities covered by the lab samples (Figure 6a) does not span the range of values seen in the full resistivity model (Fig. 6C). Therefore the drillings, which sampled sediment types other than clay, are the better traning data set with respect to extracting quick clay information from AEM models despite being less direct than lab samples.

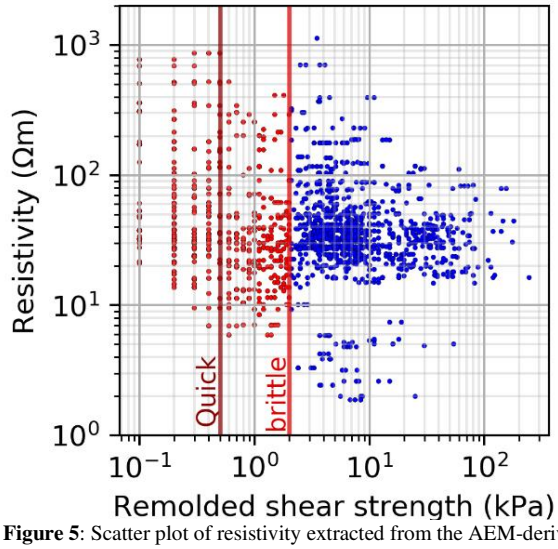

Figure 5: Scatter plot of resistivity extracted from the AEM-derived resistivity model and remolded shear strength as measured in a laboratory.

3.2.2. Classifier setup

We use a two step process to compute the probability of quick clay occurrence throughout the surveyed area. First, we classify the geotechnical drilling data using co-located lab samples as training data. Second, we use that interpretation of the drillings as input training data to classify the AEM-based resistivity model.

For the geotechnical drilling classifier, we test two different versions of the interpreter. The first "General" classifier focuses on using the general physics of the problem in such a way that it may be adaptable to other sites. It uses three attributes:

- Feed force (N),
- Vertical gradient (slope) of the feed force (N/m), and
- Depth-normalized feed-force (N/m).

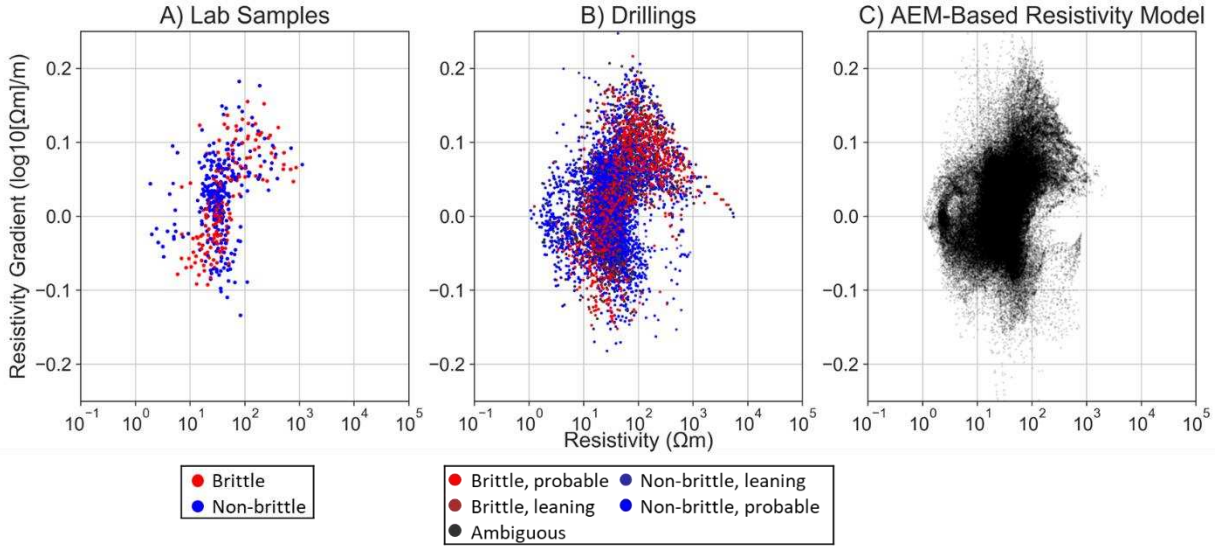

Figure 4: Scatter plots showing the spread of resistivity and resistivity gradient values in the three datasets.

A second classifier, refered to herein as the "Coordinates" classifier, uses more site-specific information by including four additional attributes:

- X-coordinate (Easting),
- Y-coordinate (Northing),
- Z coordinate (elevation), and
- Depth.

Depth is not used directly in the "General" classifier for this classifier because at this specific site, a large portion of brittle and quick material is 20-40 m depth at this field site, leading to an underestimation of quick clay at many locations where it is more shallow. Using depth-normalized feed-force is still needed in order to detect phenomena like a dry crust, where quick clay is highly unlikely to occur in the uppermost meters. Rather than raw values, the averages over a window of several meters are used. This is to account for noise from, among other things, the sudden loss of feed force every 2 m when a new drill stem segment is added.

The resistivity model classifier uses eight attributes:

- Resistivity and vertical derivatives
- X-coordinate (Easting),
- Y-coordinate (Northing),
- Z coordinate (elevation), and
- Depth.
- Elevation of surface topography

While "quick" and "brittle" can be considered separate classes in some applications, geotechnical engineers in Norway will often prioritize either material type for further investigation. Hence, we group these into a single "brittle" class throughout the rest of this paper. The geotechnical drillings classification thus becomes a two-class "brittle/non-brittle" problem. In case of the resistivity classification, some inputs have an unknown class, so the problem becomes a three-class "brittle/non-brittle/ambiguous" problem.

We experiment with several classifiers, including random forest, artificial neural networks, support vector classifiers, and Gaussian processes. We settled on random forest classifiers as our preferred method since of all the methods tested in this study, it generally yielded the best results. In addition to outputing most likely class, this classifier estimates the probability for each class. This is based on fraction of "trees" within the random forest have output have a certain label

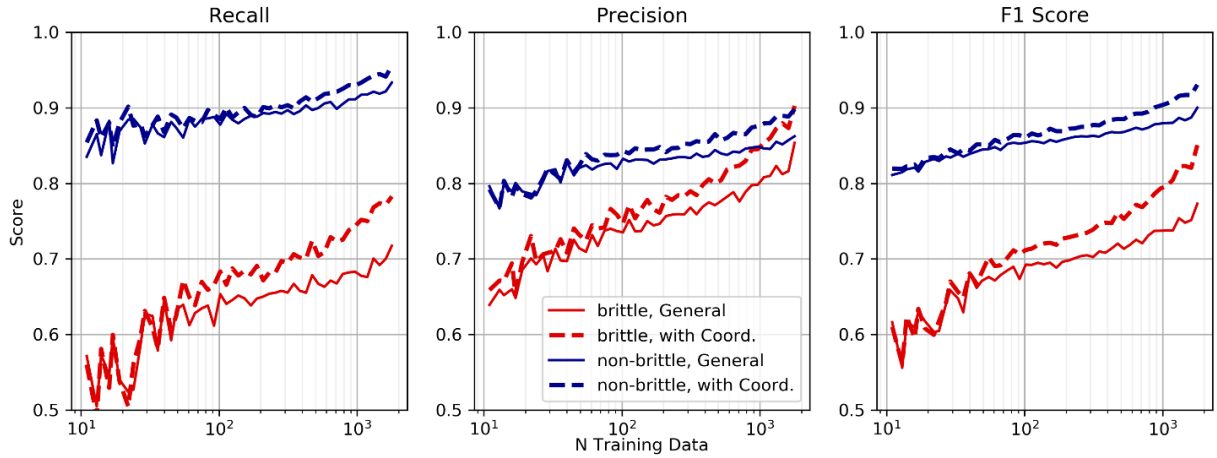

Figure 5: Performance metrics of the geotechnical sounding classifiers. Values shown are the median value of the 50 trials performed for each number of training data tested.

3.2.3. Evaluation procedure

We evaluate the performance of our classifiers by cross-validation. For each classification problem, we gradually increase the number of training data used. This is meant to simulate a workflow in a real project where new data gradually becomes available over the lifetime of a project. For the sounding classification, we use 50 different sizes of training data, ranging from 11 to 1786 of the 1922 lab sample measurements. For each test size, we input 50 random subsets of training data, running a total of 2500 trials. For the resistivity model classification, we use 40 different test sizes of trainig data, ranging from 5 to 720 of the 762 boreholes available, and 50 random subsets, leading to 2000 total trials.

Performance is gauged using three different metrics: recall, precision, and F1-Score. Recall measures what fraction of cases of a given class c were correctly identified by the classifier:

$$recall_c = \frac{TruePositives_c}{TruePositives_c + False\ Negatives_c} \quad (1)$$

$$= \frac{TruePositives_c}{TotalTrue_c} \quad (2)$$

Conversely, precision measures what fraction of predictions of a given class c by a classifier were indeed correct:

$$precision_c = \frac{TruePositives_c}{TruePositives_c + False\ Positives_c} \quad (3)$$

$$= \frac{TruePositives_c}{TotalPredictions_c} \quad (4)$$

The F1-Score is the harmonic average of the two and represents a trade-off between the two

$$F1_c = 2 * \frac{precision_c * recall_c}{precision_c + recall_c} \quad (5)$$

All three metrics have range of 0 to 1 with higher values indicating better performance.

4. Results

4.1. Geotechnical drilling interpretation

While the evaluation procedure reveals adequate performance, though there is a major imbalance between the performance metrics between brittle and non-brittle classes (**Figure 7**). At low amounts of training data, all three metrics range between 0.5 and 0.7 for brittle material. These show great improvement with increased number of training data. In contrast, non-brittle performance metrics range between 0.8 and 0.95 at the start, showing only minor improvement with increased training data. This is unsurprising given that the non-brittle class is the majority class, outnumbering the brittle class by a ratio of 2 to 1. The relationship between recall and precision also differs between the two classes. While the low recall score for brittle material indicates that more instances of brittle material are missed, the higher precision indicates that when brittle material is predicted, prediction is correct.

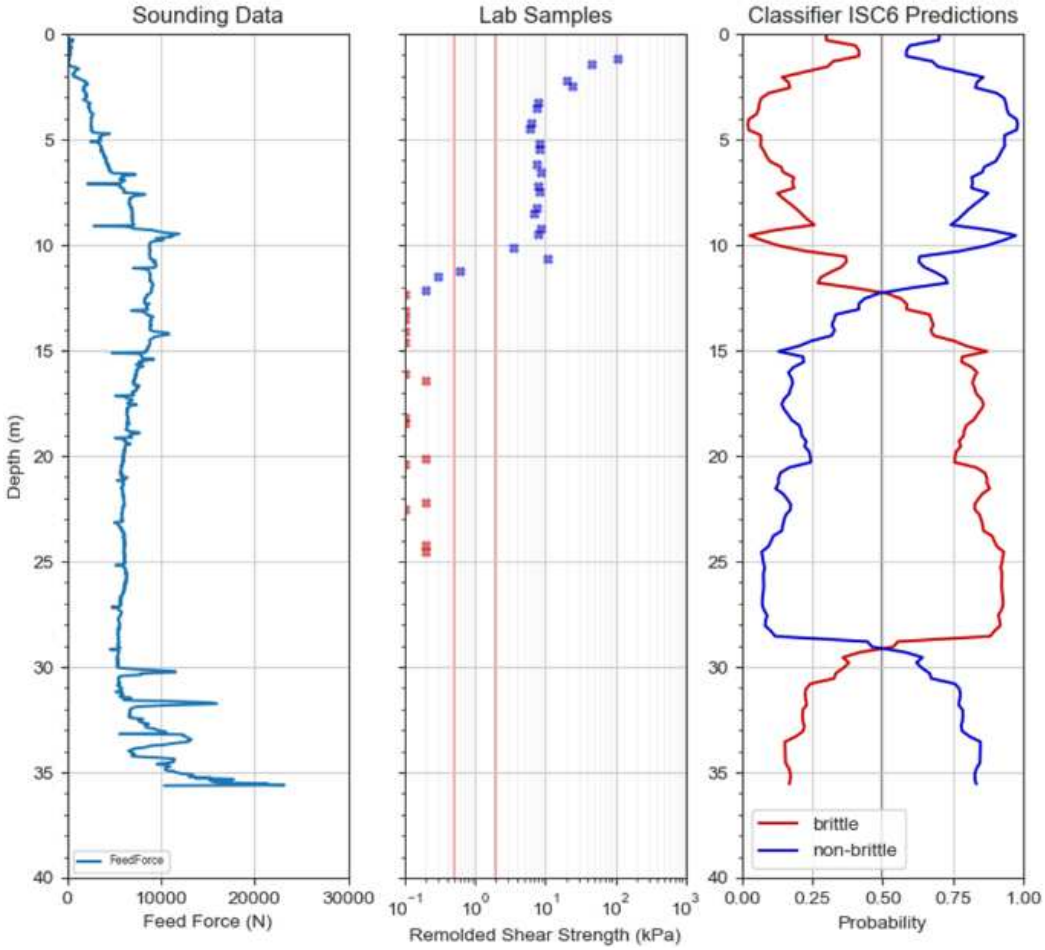

Figure 6: Example output of the General geotechnical sounding classifier where 76% of input lab samples (i.e. 1456 out of 1922) were used as training data.

The difference between the General classifier and Coordinates classifier evolves as the number of traning data increases. At low numbers of training data, there is little difference between the two classifiers, indicating that the extra geographical attributes add little information to the problem. However, as the number of training data grows, the performance of the Coordinates classifier improves relative to the General classifier, especially for the brittle class.

Inspecting some of the individual outputs manually reveals some of the areas of weakness of this method. The most prevalent issue are predictions at transition zones between brittle and non-brittle material, such as that at 11 m depth in **Figure 8**. While the classifier still correctly identifies the large body of quick clay that is over 15 m thick, it appears that using window statistics rather than

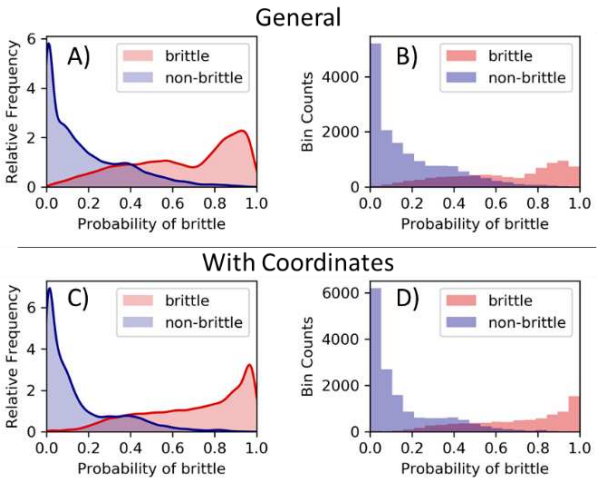

Figure 7: Distribution of probability estimates when 76% (i.e. 1456 out of 1922) of input data is used as training, seperated based on the true class.

raw values of the input attributes reduces the resolution of the output. Similarly, in some locations, the general trend of the feed force over the order of 5-10 m differs from the trend on 2m segments between each stoppage for a new drill stem (Fig. 4B).

Despite some of these weaknesses, the probability estimates attached to each prediction do give an accurate estimate of the reliability of predictions (Figure 9). Where the probability of brittle material is estimated at over 70% the prediction is almost always correct. Similarly, when the probability of brittle material is below 30%, the material is almost always non-brittle.

The final classifications of the geotechnical drillings were assigned according to the schema in **Table 1** based on the probability scores. It shows that nearly three-quarters of the soundings can be interpreted with a high degree of confidence. As with the lab sample data, the majority of borehole data are classified as non-brittle material (**Figure 10**). Brittle material still occupies a rather high proportion (roughly one quarter of the dataset), but this is not surprising given that most drillings were set up with the intent of investigating quick clay occurrence.

Table 1: Intervals used to classify the output from the geotechnical sounding interpretation.

$P_{brittle}$ Range	Interpretation
$P_{brittle} < 0.3$	Non-brittle, probable
$0.3 \leq P_{brittle} < 0.4$	Non-brittle, leaning
$0.4 \leq P_{brittle} < 0.6$	Ambiguous
$0.6 \leq P_{brittle} < 0.7$	Brittle, leaning
$0.7 \leq P_{brittle}$	Brittle, probable

For the resistivity model classification, the "leaning"

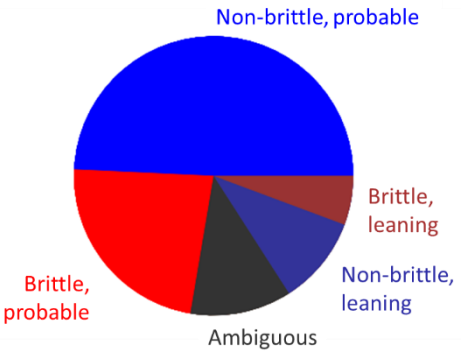

Figure 8: Proportion of the different classes found in the training data used for the resistivity model interpretation.

and "probable" labels are merged into a single class ("ambiguous") such that three classes remain in the new training dataset: "brittle/non-brittle/ambiguous"

4.2. Resistivity model interpretation

Similar to the geotechnical sounding interpretation (Figure 7), increasing number of training data has much more effect on the performance of classifying "brittle" material than "non-brittle" material from the resistivity model (Figure 11). In contrast, the differences in performance between "brittle" and "non-brittle" classification are much larger than in the previous classification problem. The median F1 Score of the brittle material does not exceed 0.5 until approximately 20 boreholes have been included as training points. In general, there is a wide spread of values for all metrics over the 50 random sets for each number of training points (indicated with the error bars in Figure 11), especially for lower numbers of training data. Additionally, the ambiguous class mostly disappears, indicating that the attributes used in classification contain little information about this class.

Despite a weak aggregate performance, other aspects of the results show some utility of this method. The probability estimates for each class still tells a similar story as in the geotechnical drilling classification problem (Figure 12). While the peak between 0.8 and 1 is not as distinct in this case in the earlier problem (Figure 9), very high probability values (0.8 to 1) and very low values (0.0 to 0.3) still indicate that the resultant classification can be trusted, even at low numbers of boreholes used as training data (Figure 12C and D). Similarly, the output grid does show the hotspots where further investigation is warranted, even if the precise geometry of the unit of senstive clay is not accurately predicted. Figure 3B shows one such example where higher resistivities of between 10 and 100 Ωm occur in the upper part of a very thick clay deposit in which the classifier correctly identifies as a unit of brittle clay.

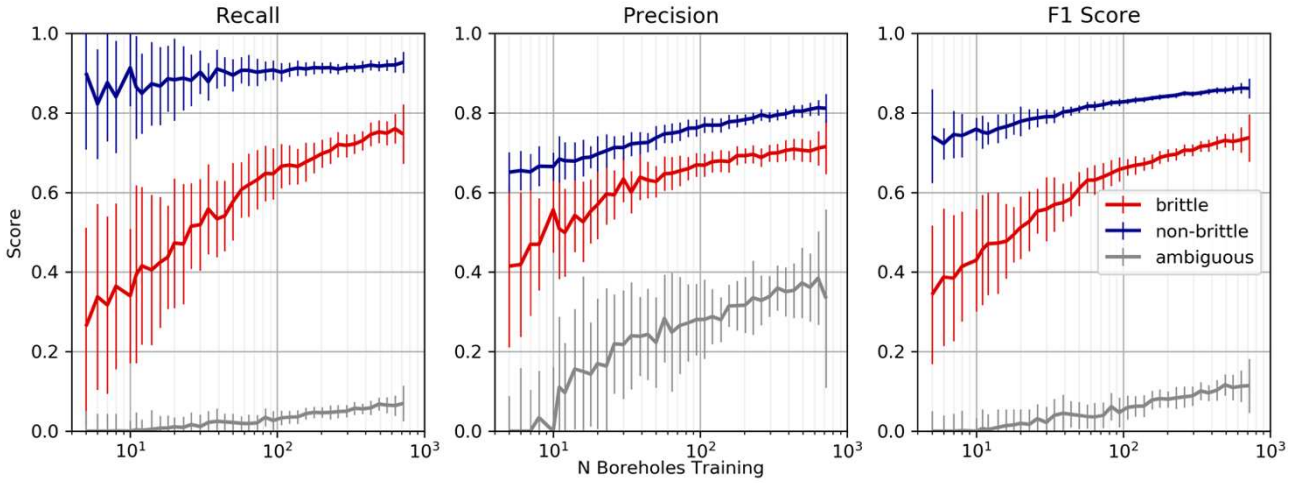

Figure 9: Performance metrics of the resistivity model classifiers. Values shown are the median value of the 50 trials performed for each number of training data tested. Error bars indicate the standard deviation.

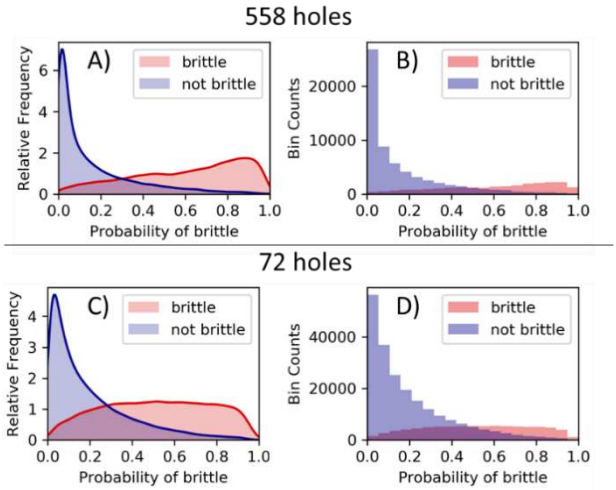

Figure 10: Distribution of probability estimates, seperated based on the true class.

5. Discussion

While these results show that, at the aggregate level, there are weaknesses in this method, we see two major strengths. First, the probability estimates allows one, even in an early project phase, to eliminate zones where brittle clay is unlikely, to confirm where it is very likely, and to indicate where there is a high degree of uncertainty. These are all helpful insight in planning follow-up site investigation. Second, this method's performance increases markedly with new training data. Being an automated method, these interpretations can be easily and quickly updated over a project's lifetime.

In addition, it is important to note that the evaluation procedure underestimates the potential utility of the method. The large error bars in Figure 11 suggest that some sets of training data are better than others. These sets were randomly chosen in this case, but in a real world project, one would be more strategic by acquiring new data where there is the greatest need for it. Further work is needed to understand what an optimal strategy for selecting new locations might be.

Based on our results, we forsee the following potential workflow for assessing brittle clay occurrence in a real-world project:

1. The General classifier is used on early geotechnical drillings to interpret soil type, with the output quality controlled by an expert
2. Those interpretations act as training data for the resistivity model classifier
3. Areas of probable brittle material and of higher uncertainty are prioritized for follow-up drilling and soil sampling
4. The geotechnical drilling classification gradually switches to the Coordinates classifier as more lab data becomes available
5. Interpretation of the resistivity model is continuously updated as new borehole and lab become available

However, there are still some unanswered questions regarding the performance of our method. For one, while the classifiers used do make errors, the more important question to ask is whether the output is an improvement over manual interpretations by an expert. Interpreting several hundred geotechnical soundings manually is a time-consuming process but is an important baseline. Second, though we expect that the General geotechnical sounding classifier would perform just as well at other sites, this should be confirmed by testing it at other sites.

In addition to these new evaluation procedures, we see a number of methodogical improvements to consider. In the case of the geotechnical sounding interpretation, better pre-processing is warranted to minimize the effect of drill stem changes and large, sudden losses in feed force. Second, rather than using statistics over a single window length, using a convoluted neural network may help with improving the detection of material boundaries. Lastly, more non-clay training points should be added. As the AEM data covers regions that are not only clay, this addition would allow for an increase in the general utility of this method.

In the case of the resistivity model classification, a generalized classifier that only uses geophysical attributes should be considered. While we hypothesize that the overall accuracy would be poorer than that our existing, site-specific one that uses spatial coordinates, it

may be useful to have a "first-pass" interpretation available right after an AEM-survey is performed but before geotechnical drillings are available. Figure 6A and B as well as work by Long et al. [11] all suggest that sediments below 5 Ωm are non-brittle, meaning that it is likely possible to identify zones of safe material even with coarse AEM data.

Lastly, the training step in both classification problems must be adjusted to account for the imbalanced data set. In both cases, the brittle class was the minority class, meaning that the training process weighs the non-brittle class more. This can be problematic depending on the aims of a particular site investigation. It may be less problematic to misclassify non-brittle material as brittle and spend extra resources to investigate it than to misclassify a potential hazardous deposit of brittle material as non-brittle and not follow-up with additional measurements. This could be addressed by trying to make the training dataset more balanced by oversampling the underrepresented class, removing data points from the overrepresented class, or by more sophisticated technices like SMOTE [17]. Alternatively, one might target the classifier training process itself. For example, one could define a cost-benefit matrix to weigh certain misclassifications more heavily than others and to compute a new performance metric: the *average utility score* [18,19]. This metric may be a more appropriate optimization target than a simple data misfit.

6. Conclusion

In summary, we have demonstrated the utility of using machine learning, airborne geophysical data, and limited intrusive geotechnical data to conduct efficient, large-scale geotechncial soil investigations. Our evaulations show that though our models' predictions are imperfect, the uncertainty attached to them have great utility in large, multi-phase soil investigations. Knowing whether sensitive clay can be ruled out, confirmed, or deemed uncertain can help guide planning for later phases, helping reduce over risk, time, and cost for a project. Our automated method can be rapidly reused to reinterpret new data, further cutting down on time needed for manual interpretation.

There remain questions about performance compared to human interpretation and about performance in other sites. We also identify areas for methodological improvements, including better improving data pre-processing and compensating for imbalanced input data.

Acknowledgement

We want to thank the Norwegian Public Road Administration for permission to use and publish the underlying field data in this study.

References

[1] Beckers, F., Chiara, N., Flesch, A., Maly, J., Silva, E. and Stegemann, U. "A risk-management approach to a successful infrastructure project", McKinsey Working Papers on Risk, Number 52, 2013.

[2] Garemo, N., Matzinger, S. and Palter R. "Megaprojects: The good, the bad and the better", McKinsey Insights, 2015.

[3] Anschütz, H.., Vöge, M.., Lysdahl, A.K., Bazin, S., Sauvin, G., Pfaffhuber, A., Bergren, A-L. "From Manual to Automatic AEM Bedrock Mapping", Journal of Environmental and Engineering Geophysics, 22(1), pp. 35-49, 2017. DOI: 10.2113/JEEG22.1.35

[4] Lysdahl, A., Pfaffhuber, A. A., Anschütz, H., Kåsing, K., and Bazin S. "Helicopter Electromagnetic Scanning as a First Step in Regional Quick Clay Mapping", In V. Thakur et al. (eds.), Landslides in Sensitive Clays, Advances in Natural and Technological Hazards Research 46, 2017. DOI 10.1007/978-3-319-56487-6_39

[5] Pfaffhuber, A. A., Anschütz, H., Ørbech, T., Bazin, S., Lysdahl, A. O. K., Vöge., M., Sauvin, G., Waarum, I.-K., Smebye, H. C., Kåsin, K., Grøneng, G., Berggren, A.-L., Pedersen J. B., Foged, N. "Regional geotechnical railway corridor mapping using airborne electromagnetics", 5th International Conference on Geotechnical and Geophysical Site Characterisation, Gold Coast, Australia, pp. 923-928. 2016.

[6] Pfaffhuber, A. A., Lysdahl, A.O.K., Sørmo, E., Bazin, S., Skurdal, G. H., Thomassen, T., Anschütz, H. Scheibz, J. "Delineating hazardous material without touching - AEM mapping of Norwegian alum shale", First Break 35, pp. 35-39, 2017.

[7] Christensen, C., Pfaffhuber, A. A., Anschütz, H., and Smaavik, T.F. "Combining airborne electromagnetic and geotechnical data for automated depth to bedrock tracking, Journal of Applied Geophysics", 119, pp. 178–191, 2015.

[8] Lysdahl, A., Andresen, L., and Vöge, M. "Construction of bedrock topography from Airborne-EM data by Artificial Neural Network", in Numerical Methods in Geotechnical Engineering, IX, pp. 691-696, 2018. DOI 10.1201/9781351003629-86

[9] Pfaffhuber AA, Lysdahl AO, Christensen C, Vöge M, Kjennbakken H, Mykland J. "Large scale, efficient geotechnical soil investigations applying machine learning on airborne geophysical models", Proceedings of the XVII European Conference on Soil Mechanics and Geotechnical Engineering, Reykjavik, Iceland, 2019.

[10] Silvestri S., Christensen C.W., Lysdahl A.O.K., Anschütz H., Pfaffhuber A.A., and Viezzoli A. "Peatland volume mapping over resistive substrates with airborne electromagnetic technology." Geophysical Research Letters, 46, 2019. Doi: 10.1029/2019GL083025

[11] Long M., Pfaffhuber A., Bazin S., Kåsin K., Gylland A., Montaflia A. "Glacio-marine clay resistivity as a proxy for remoulded shear strength: correlations and limitations", Quarterly Journal of Engineering Geology and Hydrogeology, 51, pp. 63-78, 2017. Doi: 10.1144/qjegh2016-136

[12] Sørensen, K.I. and Auken, E. "SkyTEM – A new high-resolution helicopter transient electromagnetic system", Exploration Geophysics, 35, pp. 191-199, 2004.

[13] Christiansen, A. V., Auken, E. and Sørensen, K. "The transient electromagnetic method", in Groundwater Geophysics – A tool for Hydrogeology, ed. Kirsch R, 2006. ISBN 10 3-540-29383-3

[14] Pedregosa F., Varoquaux G., Gramfort A., Michel V., Thirion B., Grisel O., Blondel M., Prettenhofer P., Weiss R. et al. "Scikit-learn: Machine Learning in Python", Journal of Machine Learning Research 12: pp. 2825-2830, 2011.

[15] Solberg I.L., Ronning J.S., Dalsegg E., Hansen L., Rokoengen K. and Sandven R. "Resistivity measurements as a tool for outlining quick-clay extents and valley-fill stratigraphy: a feasibility study from Buvika, central Norway", Canadian Geotechnical Journal 45, pp. 210–225, 2008.

[16] Bazin S. and Pfaffhuber A. "Mapping of quick clay by electrical resistivity tomography under structural constraint", Journal of Applied Geophysics 98, pp. 280–287, 2013.

[17] Chawla N.V., Bowyer K. W., Hall L. O., and Kegelmeyer W. P. "SMOTE: Synthetic minority over-sampling technique", Journal of Artificial Intelligence Research, 16(1), pp. 321-357, 2002.

[18] Baía L., and Torgo L. "Forecasting the correct trading actions", Portuguese Conference on Artificial Intelligence, Springer, Cham, Switzerland, pp. 560-357, 2015.

[19] Tinoco J, Gomes Correia A., Cortez P., and Toll D.G. Stability Condition Identification of Rock and Soil Cutting Slopes Based on Soft Computing. Journal of computing in Civil Engineering, 32(2), article number 04017088, 2018.